Quaternary Science Reviews 298 (2022) 107855

Contents lists available at ScienceDirect

Quaternary Science Reviews

journal homepage: www.elsevier.com/locate/quascirev

New multi-proxy record shows potential impacts of precipitation on the rise and ebb of Bronze Age and imperial Persian societies in southeastern Iran

Alireza Vaezi [a], Joyanto Routh [b, *], Morteza Djamali [c, e], Karolina Gurjazkaite [b], Vahid Tavakoli [d], Abdolmajid Naderi Beni [e], Patrick Roberts [f, g]

[a] Research Institute for Earth Sciences, Geological Survey of Iran, Azadi Sq, Meraj-street, Tehran, Iran
[b] Department of Thematic Studies - Environmental Change, Linköping University, Linköping, Sweden
[c] Aix Marseille Univ, Univ Avignon, CNRS, IRD, IMBE (Institut Méditerranéen de Biodiversité et d'Ecologie), Aix-en-Provence, France
[d] School of Geology, College of Science, University of Tehran, Tehran, Iran
[e] Iranian National Institute for Oceanography and Atmospheric Science (INIOAS), No. 3, Etemadzadeh Street, West Fatemi Avenue, Tehran, Iran
[f] isoTROPIC Research Group, Max Planck Institute for Geoanthropology, Jena, Germany
[g] Department of Archaeology, Max Planck Institute for Geoanthropology, Jena, Germany

ARTICLE INFO

Article history:
Received 26 August 2022
Received in revised form
16 October 2022
Accepted 2 November 2022
Available online xxx

Handling Editor: Dr Mira Matthews

Keywords:
Agriculture
Rainfall
Dynasties
Environmental proxies
Biomarkers
Pollen

ABSTRACT

The Achaemenids and Sasanian 'Persian' Empires were significant political, economic, and social forces in the Late Bronze Age and Late Antiquity Eurasia, respectively, which have left marks on the heritage of the Mediterranean and Middle Eastern world. While attention is often focused on military and political conditions when discussing the prosperity and decline of these imperial powers, their realms, which crossed a variety of environmental settings, were highly dependent on the predictability of rainfall that drove agriculture and effective provisioning. Here, we present a multi-proxy sedimentological, geochemical, and palynological record from a 2.5-m long peat deposit near the excavation site in Konar Sandal near Jiroft in southeastern Iran, covering 4000-850 cal yr BP. Around 3950 cal yr BP a wet period prevailed based on elemental ratios, stable C isotope, pollen, and diagnostic lipids. Between 3900 and 3300 cal yr BP, wet/semi-wet conditions developed with the appearance of Cerealia-type pollen. Dry and windy conditions followed (ca. 3300-2900 cal yr BP), which coincided with the Siberian anticyclones and climatic shifts developing in the Eastern Mediterranean region. Consequently, the Bronze Age settlements around Jiroft, dependent on agriculture, underwent a steady decline. A prolonged wet period followed (ca. 2900-2300 cal yr BP) with the abundance of *Sparganium*-type pollen and the aquatic lipid proxy (P_{aq}). This change coincided with intensive agricultural practices and the flourishing of the powerful Median and Achaemenid empires. The shift to high Ti/Al ratios coeval with the lowest $\delta^{13}C_{OM}$ values suggests an increase in aeolian activity and dry conditions ca. 2100-1650 cal yr BP. The Jiroft valley again experienced wet conditions between 1550 and 1300 cal yr BP, which overlapped with the economic prosperity of the middle to late Sasanian empire. The paleoenvironmental reconstruction indicates that wet periods and intensive agriculture coincide with the Persian empires' zenith, political influence, and economic affluence. Therefore, contextualized and detailed paleoenvironmental records are desirable to explore the interplay of political and climatic factors in the development and fragmentation of the ancient settlements and imperial powers in Eurasian history.

1. Introduction

Iran was at the center of significant political and economic developments from the Bronze Age to Late Antiquity (Touraj, 2012; Colburn, 2013; Mashkour et al., 2013; Djamali et al., 2016; Sharifi et al., 2015; Clarke et al., 2016; Petrie and Weeks, 2019). During

* Corresponding author.
E-mail address: joyanto.routh@liu.se (J. Routh).

https://doi.org/10.1016/j.quascirev.2022.107855

the Early Bronze Age (EBA) period, expanding settlements, such as those found in the Jiroft Valley from the 3rd millennium BC (Madjidzadeh and Pittman, 2008; Mashkour et al., 2013; Gurjazkaite et al., 2018) saw people, and increasingly intensive agricultural activities, congregate around river valleys. A gradual transition materialized from isolated nomadic lifestyles to urban communities focused on agriculture, trade, and commerce. This trend followed the emergent Mesopotamian urban world of the 4th millennium BC and extended further east (Staubwasser and Weiss, 2006; Mancini-Lander, 2009; Petrie and Weeks, 2019). In the Jiroft Valley, significant Bronze Age occupation phases have been identified at "Konar Sandal South" (KSS), which seems to have declined ca. 4200 cal yr BP due to desertification (Madjidzadeh and Pittman, 2008; Fouache et al., 2009; Fallah et al., 2015; Gurjazkaite et al., 2018), and "Konar Sandal North" (KSN), which is dated to be around the end of the 2nd millennium BC and the beginning of the 1st millennium BC (Mashkour et al., 2013). The economy of these Bronze Age societies was based on the cultivation of cereals (barley, wheat), fruits (dates, grapes), and herding (sheep, goats, and cattle). Favorable climatic conditions for agriculture prevailed in these dry landscapes bordering the deserts. Jiroft became a significant part of the expanding Bronze Age trade routes between the Indus Valley, the Iranian plateau, the Persian Gulf, and Mesopotamia (Madjidzadeh and Pittman, 2008; Fouache et al., 2009; Mashkour et al., 2013; Vidale and Frenez, 2015; Petrie and Weeks, 2019). Notably, these EBA settlements in southeastern Iran (Tapeh Yahya, Bampur, Shahr-e sokteh, Shahdad, Tal-i Iblis, and others) started developing into proto-urban communities as the population swelled (Pyankova, 1994; Colburn, 2013; Petrie and Weeks, 2019). The close association between agriculture and water and involvement in the more expansive Eurasian exchange systems established during the EBA set the tone for political influence and economic growth in Jiroft. The Iron Age followed the EBA settlements in this region, which saw the emergence of urban centers with distinct styles, architecture, and cultural development. Then came the Achaemenid Empire, the largest empire in history at its time (Turchin et al., 2006; Touraj, 2012; Colburn, 2013), and, later, the Sasanians, one of the primary challengers to Roman imperial ambitions in the east (Mancini-Lander, 2009; Shumilovskikh et al., 2017).

The fate of subsequent political forces, including the Achaemenid and Sasanian Empires, has been linked to weak successions, nomadic attacks, settlement decentralization, and disease (Madella and Fuller, 2006; Fouache et al., 2009; Mashkour et al., 2013). However, it has also been suggested that mid-to-late Holocene climate change may have heavily impacted agriculture and provisioning at the core of these imperial structures in the middle east (Clarke et al., 2016). Consistent with this, a medley of mid-to-late Holocene climatic and land-use changes swept through the region (Mashkour et al., 2013; Fallah et al., 2015; Sharifi et al., 2015; Petrie and Weeks, 2019). However, these human-environment interactions have generally been neglected relative to the extended discussions of military conquests and political achievements. This limits our understanding of how climate change interacted with the imperial power's manifestations (or not) in agriculture, economic exchange, settlement, and political control at different points in space and time. Recent studies indicate complex interactions between the southwest Indian Ocean Summer Monsoon (IOSM), Mid-Latitude Westerlies (MLW), and the northeast Siberian Anticyclone in the southeastern Iranian Plateau, which had a lasting impact on Iranian landscapes (Sharifi et al., 2015; Fallah et al., 2015; Hamzeh et al., 2016; Vaezi et al., 2019). These studies indicate that Jiroft and other Bronze Age settlements in southeastern Iran declined steadily during the late Holocene, a time of reduced monsoon activity and rainfall (Madjidzadeh and Pittman, 2008; Mashkour et al., 2013; Gurjazkaite et al., 2018). However, the near absence of high-resolution palaeoclimate and palaeoenvironmental records in the region has triggered debates. Nonetheless, the potential vulnerability of the early settled communities and states to natural calamities such as droughts, floods, and famines driven by climate change has been proposed from Mesopotamia to China (Weiss et al., 1993; Staubwasser and Weiss, 2006; Zhang et al., 2008; Ponton et al., 2012; Dixit et al., 2014; Sharifi et al., 2015; Clarke et al., 2016; Sinha et al., 2019; Petrie and Weeks, 2019; Laskar and Bohra, 2021). Here, the debate is not so much about whether climate impacted ancient states and settlements but rather to what extent it influenced economic prosperity and political control relative to other factors. The narratives in which these questions and responses are presented should be further tested as hypotheses.

The ancient Jiroft Valley, situated in a transitional zone between the semi-arid region to the north and the arid areas to its south, is a promising site for paleoclimate studies to reveal climate fluctuations and their potential influence on human societies in the wider Iranian region (Gurjazkaite et al., 2018; Vaezi et al., 2019). The region's proximity to the deserts (e.g., Dasht-e Lut) would have made its environments and societies particularly sensitive to climate change in the past (Fallah et al., 2015; Vaezi et al., 2019). Recent studies focused on a peat deposit near the EBA excavation center in Konar Sandal (KSN, Jiroft) and a dry ephemeral playa ca. 100 km to its south have highlighted the potential of multi-proxy records from the region to yield insights into climate and environmental changes in the vicinity of key historical records of human behavior. Precipitation changed from a monsoon-dominated (IOSM) regime to one influenced by the MLW during the mid-to-late Holocene (Vaezi et al., 2019; Safaierad et al., 2020). While the Saharo-Sindian open pseudo-savanna vegetation dominated Konar Sandal for ca. 4000 years, agro-pastoral activities and climatic factors changed the land cover from open xeric scrubland to a degraded landscape (Gurjazkaite et al., 2018).

In this study, we reconstruct the paleoclimatic and palaeoenvironmental history in southeastern Iran by tracing landscape changes and climate fluctuations from the Late Bronze Age into Late Antiquity. We produce a multi-proxy paleoenvironmental record in a 250-cm long peat sequence extracted near the archaeological complex at Konar Sandal (KSN) near Jiroft, covering the last 4000 cal yr BP. Combining sedimentological, geochemical, and paleoecological proxies, including biomarker analyses, we explore paleoenvironmental changes in the region and evaluate their possible effects on the EBA settlements and major ruling dynasties of Iran based on archaeological and historical records of territorial boundaries, economic prosperity, and political changes. The multi-proxy data suggest significant shifts in the peat deposit at different time intervals. These changes connected to shifts in vegetation cover, agricultural practices, and water level fluctuations around Konar Sandal are not isolated but have broad parallels in the Holocene paleoenvironmental and historical records in Iran and in tracing the rise and ebb of the imperial dynasties that ruled the region.

2. Geographical setting

Konar Sandal (25 km south of Jiroft in southeast Iran) is the most significant archaeological excavation site in the Halil Rud Valley. Several high mountain chains surround it, some rising to 3700 m asl (Fig. 1A). The location is close to the margin of the Inter-Tropical Convergence Zone (ITCZ), making it extremely sensitive to the position of the ITCZ and its migration. The Halil Rud stretches from north to southeast for almost 400 km through fertile agricultural land before draining into the Jazmurian playa southeast of Konar Sandal. The water level in the river fluctuates depending on the

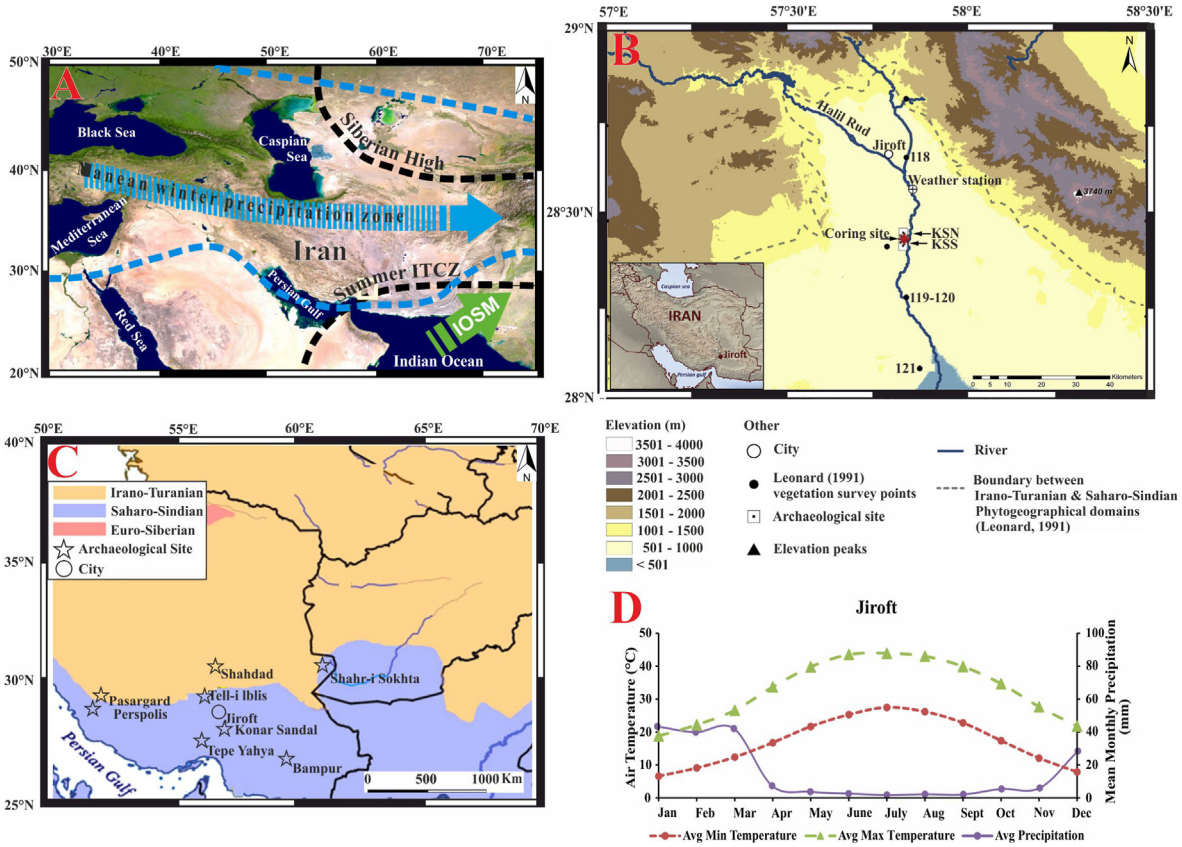

Fig. 1. Major climate systems over West Asia (Vaezi et al., 2019) and the location of the Jiroft Valley in southeastern Iran. A) dotted lines indicate the approximate current location of the Intertropical Convergence Zone (ITCZ), Mediterranean winter precipitation limits, and the Siberian Anticyclone; IOSM refers to the Indian Ocean Summer Monsoon, and the white rectangle indicates the study area, B) The Jiroft Valley and its major physical, archaeological, and phytogeographical features. The location of the peat deposit in this study is situated between the two excavation sites, Konar Sandal North (KSN) and Konar Sandal South (KSS) (Gurjazkaite et al., 2018), C). Phytogeographic boundaries after White and Léonard, (1991) and positions of archaeological sites near the study area, and D), a 30-years average of the minimum and maximum monthly mean air temperature (°C) and monthly precipitation (mm) as recorded in the Jiroft weather station.

annual precipitation. The playa is covered by Quaternary sediments such as sandstone, conglomerate, marl, and gypsum (Shirani et al., 2020; Zandifar et al., 2022).

Eocene pyroclastic rocks with intercalations of calcareous sandstone and sand-bearing limestone dominate the area. Granites, granitoid, and acid to mafic dikes also occur in the region, forming elevated areas (Faraji et al., 2019). Low to medium-grade metamorphic rocks consisting of chlorite formed by thermal metasomatism is found widely (Emami et al., 2017). These outcrops were probably the source of raw materials for the archaeological stone artifacts recovered from Jiroft (Emami et al., 2017). There is a gently sloping gravel plain between the mountains (Jebel Barez in the northeast and the Sardouyeh in the northwest) and the alluvial flood plains (Fouache et al., 2005). Two raised structures (KSN and KSS, Fig. 1B) and an urban housing complex were excavated next to the riverbed (Madjidzadeh and Pittman, 2008). Also, lying close by is the cemetery of Mahtutabad, which the Halil Rud flooded in 1999, exposing the Bronze Age artifacts consisting of steatite vessels, pottery, jewelry, and other artifacts (Madjidzadeh and Pittman, 2008). Close to Konar Sandal are other EBA settlements where excavations have been going on for several decades, e.g., Tepe Yahya and Shahdad (Fig. 1 C).

The Jiroft Valley lies on the boundary of the Irano-Turanian and the Saharo-Sindian phytogeographical regions (Leonard, 1993; Gurjazkaite et al., 2018, Fig. 1B and C). The southern side of the plains falls within the Saharo-Sindian region, whereas the northern side has Irano-Turanian flora (Agnew and Zohary, 1974; Leonard, 1993; Gurjazkaite et al., 2018). The study area has relict stands of degraded forest vegetation, and near Konar Sandal, the vegetation is dominated by spiny shrubs resulting from overgrazing (Gurjazkaite et al., 2018) and dry conditions. However, the floodplains around Konar Sandal have flourishing agriculture, and vast tracts of land are covered with cereal (wheat, barley), date palm, and citrus plantations, as well as the ruderal vegetation associated with cultivated land.

3. Materials and methods

3.1. Sampling, magnetic susceptibility, and grain size analysis

Two cores, labeled Dar-1 and Dar-2, with lengths of ca. 2.5 and 1.9 m, were retrieved using a Russian peat borer. All the analyses were done on Dar-1 and the Dar-2 core was archived for future investigations. The deposit lies between the raised archaeological mounds at Konar Sandal from a spot named Daryache (Persian name for lake), 25 km south of the modern city of Jiroft (27°37′04″ N, 58°34′77″ E; Fig. 1). The core was logged in the field, photographed, and later stored at 4 °C and constant humidity at the Iranian National Institute for Oceanography and Atmospheric Science (INIOAS) Marine Geology Laboratory. The intact core was

passed through an MS2C Bartington magnetic susceptibility (MS) meter (sensitivity of about 2×10^{-6} SI) and measured at 2-cm increments. The cores were then transported to Linköping University in Sweden, where the longer Dar-1 core was sliced at 1-cm intervals and freeze-dried. The grain size was measured every 1–4 cm in the freeze-dried sediments using a Micromeritics SediGraph III Particle Size Analyzer. An ultrasonic stirrer was used for 30 s to prevent flocculation. Repeated measurements were carried out for a few select samples to calculate the instrument precision.

3.2. Radiocarbon analyses

Based on variations in the sediment characteristics (lithology, MS, and grain size), eight sub-samples were submitted for radiocarbon (^{14}C) analysis to the Poznań Radiocarbon Laboratory (see details in Gurjazkaite et al., 2018). In general, samples were combusted with CuO and Ag wool at 900 °C for 10 h, and CO_2 produced was reduced to pure graphite in a vacuum-sealed line (Goslar et al., 2004). Coal or IAEA C1 Carrara Marble and Oxalic Acid II standards were subjected to the same pre-treatment and combustion procedures. The ^{14}C content in samples was measured using Compact Carbon Accelerator Mass Spectrometry (AMS) as per Goslar et al. (2004). The conventional ^{14}C age was calculated using a correction factor for isotopic fractionation described by Stuiver and Pollach (1977). The age data were extrapolated within a Bayesian framework using the BACON software package (Blaauw and Andrés Christen, 2011). BACON divides the core into vertical sections and uses Markov Chain Monte Carlo (MCMC) iterations to estimate the accumulation rate (years/cm). ^{14}C dates were calibrated using the Intcal 20 calibration curve (Reimer et al., 2020).

3.3. Elemental and mineralogical analyses

X-ray fluorescence (XRF) analysis was conducted at intervals of 1–5 cm with a hand-held XRF scanner (S1 TITAN, Bruker) equipped with a rhodium X-ray tube and XFlash® Silicon Drift Detector (SDD). The mass % unit was estimated using the Geochem Trace program. Scanning was performed at 1 min/scan. In addition, 22 sub-samples covering the entire length of the peat were selected for major and trace element analysis using an Inductively Coupled Plasma Mass Spectrometer (PerkinElmer NexION 300) to verify the XRF results. For extracting the metals, a pseudo-total digestion method using 10 mL of HNO_3 acid (14 M) was added to 0.3 g sediments and digested by a Microwave Milestone Ethos 1 digester. Reference standard from the National Research Council of Canada (PACS-2) was analyzed with the samples to assess the precision and accuracy. Analytical precision based on three replicates was within ±5% of the suggested values.

3.4. C/N and stable isotope analyses

Forty-three freeze-dried, acid-treated sediment samples (fumigation method; Hedges and Stern, 1984) were analyzed for organic C and N concentrations and $\delta^{13}C$ and $\delta^{15}N$ measurements. The analyses were done at the Stable Isotope Mass Spectrometry Laboratory, University of Florida, using a Carlo Erba Elemental Analyzer NC1500 attached to a Thermo Electron DeltaV Advantage gas-ratio mass spectrometer. Calibration was based on repeated measurements of NBS-19 and internal standards. The analytical precision based on replicate analyses of standards were C ± 0.04% and ±0.05‰ and N ± 0.006% and 0.08‰, respectively. The C/N value was reported as a mass ratio; the $\delta^{13}C_{OM}$ was reported in conventional delta (δ) notation vs. V-PDB.

3.4.1. Lipid extraction

Approximately 5–6 g of freeze-dried peat sample was extracted with a mixture of CH_2Cl_2 and MeOH (9:1 v/v) using an accelerated solvent extractor (Dionex ASE 300; 3 cycles at 1000 psi and 100 °C). The extracts were reduced using a Büchi SPE extractor, and half the volume was stored for archival purposes. Next, the lipid fractions were separated using the solid phase extraction technique using aminopropyl (LC-NH_2) cartridges (see Njagi et al., 2021). The n-alkanes were eluted with 5 mL hexane before reducing under pressure and concentrated to dryness under nitrogen. The extracts were then re-dissolved in hexane and spiked with deuterated tetracosane and androstane (internal standards). The samples were analyzed using an Agilent 6890 N gas chromatograph (GC) interfaced with a 5973 MSD mass spectrometer (MS) with an HP-5 (5% phenyl methyl siloxane) fused silica capillary column (30 m length x 0.25 mm i.d. x 0.25 μm film thickness). The oven was kept at a constant temperature of 35 °C for 6 min, increased to 300 °C at 5 °C min^{-1} and then held for 20 min. The GCMS was operated at 70 eV in full scan mode (*m/z* 50–500 amu). The compounds were identified based on authentic standards, their retention time, *m/z* ratios, and major ion fragments indicated in the NIST and Lipid library. The detection limit of compounds ranged from 0.1 up to 1 ng/g. Recovery of the deuterated hexatriacontane ranged from 75 to 85%.

n-Alkanes extracted from organic matter present in samples were used to calculate the input of odd-numbered high molecular weight compounds (C_{27}, C_{29}, and C_{31}) and various n-alkane ratios such as P_{aq}, Average Chain Length (ACL), Carbon Preference Index (CPI), and Terrigenous Aquatic Ratio (TAR) for tracing the characteristics of organic matter sources in the peat deposit. The ratios used for calculating P_{aq}, CPI, TAR, and ACL were:

(Ficken et al., 2000)

$$\mathrm{Paq} = \frac{(\mathrm{C23} + \mathrm{C25})}{(\mathrm{C23} + \mathrm{C25} + \mathrm{C29} + \mathrm{C31})} \quad (1)$$

(Allan and Douglas, 1977)

$$\mathrm{CPI} = \frac{\sum(\mathrm{C23} - \mathrm{C31})\mathrm{odd} + \sum(\mathrm{C25} - \mathrm{C33})\mathrm{odd}}{2\sum(\mathrm{C24} - \mathrm{C32})\mathrm{even}} \quad (2)$$

(Bourbonniere and Meyers, 1996)

$$\mathrm{TAR} = \frac{(\mathrm{C27} + \mathrm{C29} + \mathrm{C31})}{(\mathrm{C15} + \mathrm{C17} + \mathrm{C19})} \quad (3)$$

(Eglinton and Hamilton, 1967)

$$\mathrm{ACL} = \frac{(25\mathrm{C25} + 27\mathrm{C27} + 29\mathrm{C29} + 31\mathrm{C31} + 33\mathrm{C33})}{(\mathrm{C25} + \mathrm{C27} + \mathrm{C29} + \mathrm{C31} + \mathrm{C33})} \quad (4)$$

3.5. Pollen analysis

Pollen extraction and identification were performed on thirty-five subsamples at 1–10 cm intervals at the Institut Méditerranéen de Biodiversité et d'Ecologie (IMBE), Aix-en-Provence, France. A detailed interpretation of pollen data is already presented in a previous publication by Gurjazkaite et al. (2018). In this study, the pollen-based vegetation reconstructions are cross-correlated with the new geochemical data and re-interpreted to support the multi-proxy paleoenvironmental reconstructions, focusing on tracking rainfall changes which are tricky to identify based on pollen analysis alone.

Proxies used to interpret the palaeoenvironmental conditions in this study are summarized in Table 1.

Table 1
Summary of paleoenvironmental proxies and their interpretation.

Environmental proxy	Interpretation	Environmental proxy	Interpretation
Sand content and Magnetic susceptibility (MS)	High MS with elevated sand content supports the presence of a high-energy environment (Jiang and Ding, 2010).	P_{aq}	P_{aq} ratio is based on the abundance of mid-chain n-C_{23} and C_{25} alkanes. The value 0.4 < Paq <1.0 corresponds to submerged/ floating macrophytes (Ficken et al., 2000). Higher values suggest more aquatic plant input.
Si/Al, Ti/Al	Higher Ti/Al and Si/Al ratios signify an increase in aeolian input, which means dry conditions (Calvert and Fontugne, 2001; Mercone et al., 2001; Martinez-Ruiz et al., 2015).	Carbon Preference Index (CPI)	High values indicate higher terrestrial plant sources and better preservation of OM (Cranwell et al., 1987).
Fe/Al	Increases in the Fe/Al ratio indicate episodic drought (Martinez-Ruiz et al., 2015; Mercone et al., 2001).	Terrigenous Aquatic Ratio (TAR)	Higher concentrations of long-chain (n-C_{29}, C_{31}) alkanes and higher terrigenous aquatic ratio (TAR) are characteristic of terrestrial vegetation (Bourbonniere and Meyers, 1996).
K/Ti	High K/Ti suggests an increase in chemical weathering and higher alluvial inputs (Wehausen and Brumsack, 2000; Martinez-Ruiz et al., 2015)	Average Chain Length (ACL)	ACL values respond more strongly to changes in water level. A decrease in ACL can be linked to wet conditions (Cranwell, 1974; Schwark et al., 2002).
TOC	High values suggest a high input of OM and good preservation.	*Sparganium*-type pollen	More *Sparganium*-type pollen (Typhaceae family) than other aquatic plants (Cyperaceae in this study) suggests a higher water table in the wetland (e.g. (Aubert et al., 2017; Djamali et al., 2008)
C/N ratio	High values suggest terrestrial input. Low values imply poor preservation from microbial/chemical degradation or low organic input (Meyers, 1997).	*Artemisia,* Ephedraceae, and *Calligonum*	Abundance of *Artemisia* means dry conditions and desertification (Dehghani et al., 2017). Ephedraceae *and Calligonum* are an indicator of desertification and the development of dunes (Djamali et al., 2008).
$\delta^{13}C_{OM}$	High values indicate higher productivity and freshwater availability (Enzel et al., 1999)	Cerealia-type pollen	The abundance of *Cerealia*-type pollen indicates more intensive agricultural practices.

4. Results

4.1. Age-depth model and chronology

Eight ^{14}C dates were used to establish the 250-cm long peat chronology. Except for a slight offset in the sample at 245 cm (by less than a century), all other samples are in a chronological sequence extending to 4011 cal yr BP at the bottom of the peat sequence. (Fig. 2). Based on the age-depth model, the two highest sedimentation rates (2.04 and 1.76 mm/yr) occurred between 250 cm and 195 cm. The lowest SR (0.33 mm/yr) occurred between 35 cm and the top of the core. The chronology shows that the peat sequence spans important historical events since the projected collapse of EBA Jiroft at ca. 4200 cal yr BP, followed by the Iron Age, the Persian Empires (550 BCE-650 CE), and finally ending during the middle of the Islamic period.

4.2. Units

The sediment core was divided into six major units based on its sedimentological, geochemical, and palynological characteristics (Fig. 3; also see supplementary data Figs. 1 and 2).

4.2.1. Unit 1 (U 1; 250-189 cm; ca. 4000-3550 cal yr BP)

Unit 1 extended from the bottom of the peat sequence to 189 cm, corresponding to the period ca. 4000 cal yr BP to 3550 cal yr BP (Fig. 3). This unit had high sand content (~75%), and MS (30 SI) compared to other sections in the core. Si, Al, and K had high values around 245 cm and then gently decreased towards the top of this unit. The elemental ratios (Si/Al, Ti/Al, and Fe/Al) had low values in Unit 1. The exception was the peat horizon at ca. 3650 cal yr BP (200 cm), where Ti/Al increased rapidly. The $\delta^{13}C_{OM}$ exhibited some of the lowest (−25.3 to −25.0‰) values. TOC increased, and the C/N ratio had the highest value (19) at ca. 3660 cal yr BP. The $\delta^{15}N$ values were low in this unit compared to the others. TAR reached the highest values at ca. 3900 cal yr BP and remained high until the middle of this unit. The first significant appearance of Cerealia-type pollen occurred in this unit extending from 3880 to 3700 cal yr BP (230-207 cm). The distinctive peaks of long-chain (n-C_{29}, C_{31}) alkanes (see Fig. 2, supplementary data) and *Artemisia* occurred ca. 3800 cal yr BP (220 cm). From 3800 cal yr BP, there is an increase in *Sparganium*-type pollen (reflecting the family Typhaceae associated with vegetation on the margins of a pond) and a sharp decline in *Artemisia* and long-chain n-alkanes towards the top of this unit.

4.2.2. Unit 2 (U 2; 189-164 cm; ca. 3550-3300 cal yr BP)

In unit 2, sand content gradually increased upwards, the peat was degraded, and its low TOC content characterized it. MS was low (5 SI), and concentrations of Si, Al, and K were low in the mid-section of this unit before they increased. The $\delta^{13}C_{OM}$ showed a distinct increase in this unit and exhibited higher values (−20.70‰). C/N ratios sharply declined and had lower values than Unit 1. In this unit, *Artemisia,* long-chain (n-C_{29}, C_{31}) alkanes, ACL, and TAR were low. However, Cerealia-type pollen had low values in this unit. The exception was the sediment horizon at ca. 3400 cal yr BP (174 cm), where Cerealia-type pollen was relatively high along with P_{aq}.

4.2.3. Unit 3 (U 3; 164-134 cm; ca. 3300-2900 cal yr BP)

Unit 3 was characterized by high sand content (92.7%). The elemental ratios (Si/Al, Ti/Al, and Fe/Al) have higher values than the other units. Si/Al and Fe/Al ratios reached their highest values at ca. 3200 cal yr BP (154 cm). TOC and TN were overall low and did not show significant shifts in their trends. The $\delta^{13}C_{OM}$ showed a sharp decrease from the beginning of this unit until ca. 3200 cal yr BP. Unit 3 had higher C/N than Unit 2 and was also characterized by the highest counts of *Artemisia*. The highest ACL values were coeval with the deposition of long-chain (n-C_{29}, C_{31}) alkanes and TAR in this unit. This unit indicated the low pollen counts of Typhaceae (*Sparganium*-type). Also, Cerealia-type pollen demonstrated the lowest counts in this unit.

4.2.4. Unit 4 (U 4; 134-106 cm; ca. 2900-2300 cal yr BP)

Unit 4 consisted predominantly of sand (93.7%). The high values of elements (Si, Al, K) were accompanied by low values of geochemical ratios (Si/Al and Ti/Al). The K/Ti ratio had the highest values in the entire core in this unit. The results showed very low

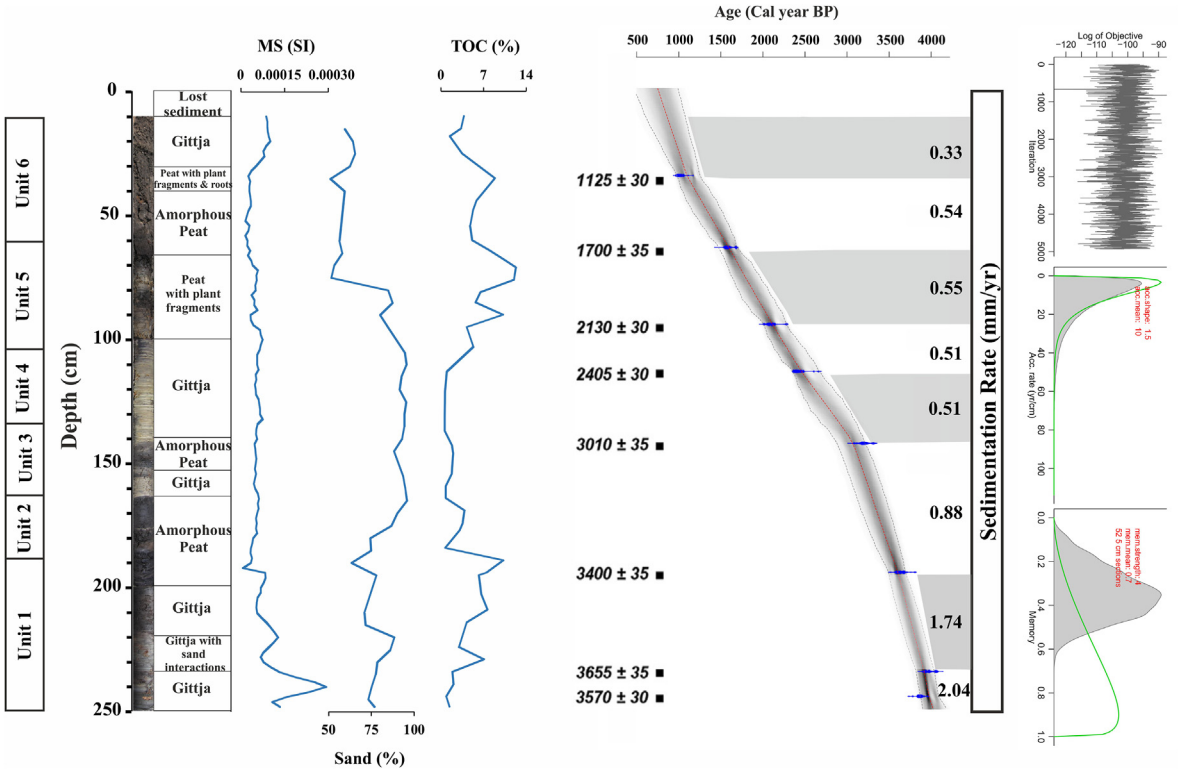

Fig. 2. Age-depth model and lithology in the Daryache peat sequence, Jiroft (southeastern Iran). The visual characteristics of the 2.5-m peat sequence, lithology, chronology, and depth are included. In addition, the sedimentological trends are plotted vs. depth. The units (Unit 1–6) represent shifts in sedimentological and geochemical properties. Age-depth model was generated for the peat deposit based on eight calibrated radiocarbon dates using the BACON (Blaauw and Andrés Christen, 2011) and IntCal 20 (Reimer et al., 2020). The calibrated 14C dates (transparent blue) and the age-depth model (darker grey indicate more likely calendar ages and grey stippled lines infer 95% confidence intervals) are shown on the figure's right. (For interpretation of the references to colour in this figure legend, the reader is referred to the Web version of this article.)

values of TOC (0.74%), C/N ratios (7.6), long-chain n-alkanes, CPI, and TAR in this unit. The $\delta^{13}C_{OM}$ became lower (−23.9‰) before it increased near the top of the unit. This unit was characterized by the highest P_{aq} and lowest ACL values. The bottom of Unit 4 is characterized by the decline in *Artemisia*, followed by a decrease towards the top. *Sparganium*-type pollen counts had the highest values in this unit. Towards the top of this unit, there is a gradually decreasing trend of *Sparganium*-type pollen. There is a continuous presence of Cerealia-type pollen in this unit.

4.2.5. Unit 5 (U 5; 106-61 cm; ca. 2300-1550 cal yr BP)

There is an overall decrease in the amount of sand in this unit. Ti/Al had a high and increasing trend in the core. K/Ti had low values. There is the presence of plant fragments in the sediments. The $\delta^{13}C_{OM}$ values were low in Unit 5, with a mean value of around −23.1‰. C/N had high values. The absence of Cerealia-type pollen characterized the start of this unit, but then it increased until the mid-section, followed by a decrease. Typhaceae and *Artemisia* did not show many changes in their trends. Cyperaceae and pollen counts representing trees and shrubs increased gradually before decreasing toward the top of this unit (Fig. 3).

4.2.6. Unit 6 (U 6; 61-10 cm; ca. 1550-850 cal yr BP)

Unit 6 was characterized by low sand content (~40%) and a slight increase in MS near the top. The unit has moderate values of elemental ratios. The exception was the sediment horizon at ca. 1075 cal yr BP (34 cm), where Si/Al and Ti/Al were higher. The $\delta^{13}C_{OM}$ showed some fluctuations between 1350 and 1200 cal yr BP followed by a gradual decrease towards the top of the unit. The $\delta^{15}N$ values were high (4.7–6.7‰) near the core top. Artemisia percentages were low in this unit, and there was a moderate presence of *Sparganium*-type pollen. There were lower Cerealia-type pollen counts compared to the units below.

5. Discussion

5.1. Paleoclimate preceding the decline of the Jiroft civilization

Unit 1 (250-189 cm, ca. 4000-3550 cal yr BP) and Unit 2 (189-164 cm, ca. 3550-3300 cal yr BP) coincide with paleoclimate changes consisting of mostly wet/semi-wet conditions punctuated by two short dry spells before the Jiroft EBA settlement entered a steady decline ca. 3200 cal yr BP. Unit 1 coincides with the highest sedimentation rate coeval with high MS and relatively high sand content at the base of the peat sequence. This deposition trend implies a high-energy environment (Jiang and Ding, 2010, Fig. 2). Near the bottom, Gurjazkaite et al. (2018) infer flooding by the Halil Rud based on the high MS. The low Ti/Al and Si/Al ratios signify a decreased aeolian input, which means that the climate was probably wet and humid (Calvert and Fontugne, 2001; Mercone et al., 2001; Martinez-Ruiz et al., 2015). Consistent with this interpretation, high K/Ti during this interval suggests increasing chemical weathering and higher alluvial inputs (Wehausen and Brumsack, 2000; Martinez-Ruiz et al., 2015). The availability of high freshwater input could result in higher $\delta^{13}C_{OM}$ values during wet periods in otherwise dry areas, as observed in the playas in western India (Enzel et al., 1999). Based on this evidence and the low C/N values, it is likely that wet conditions existed at ca. 3950 cal yr BP in Jiroft.

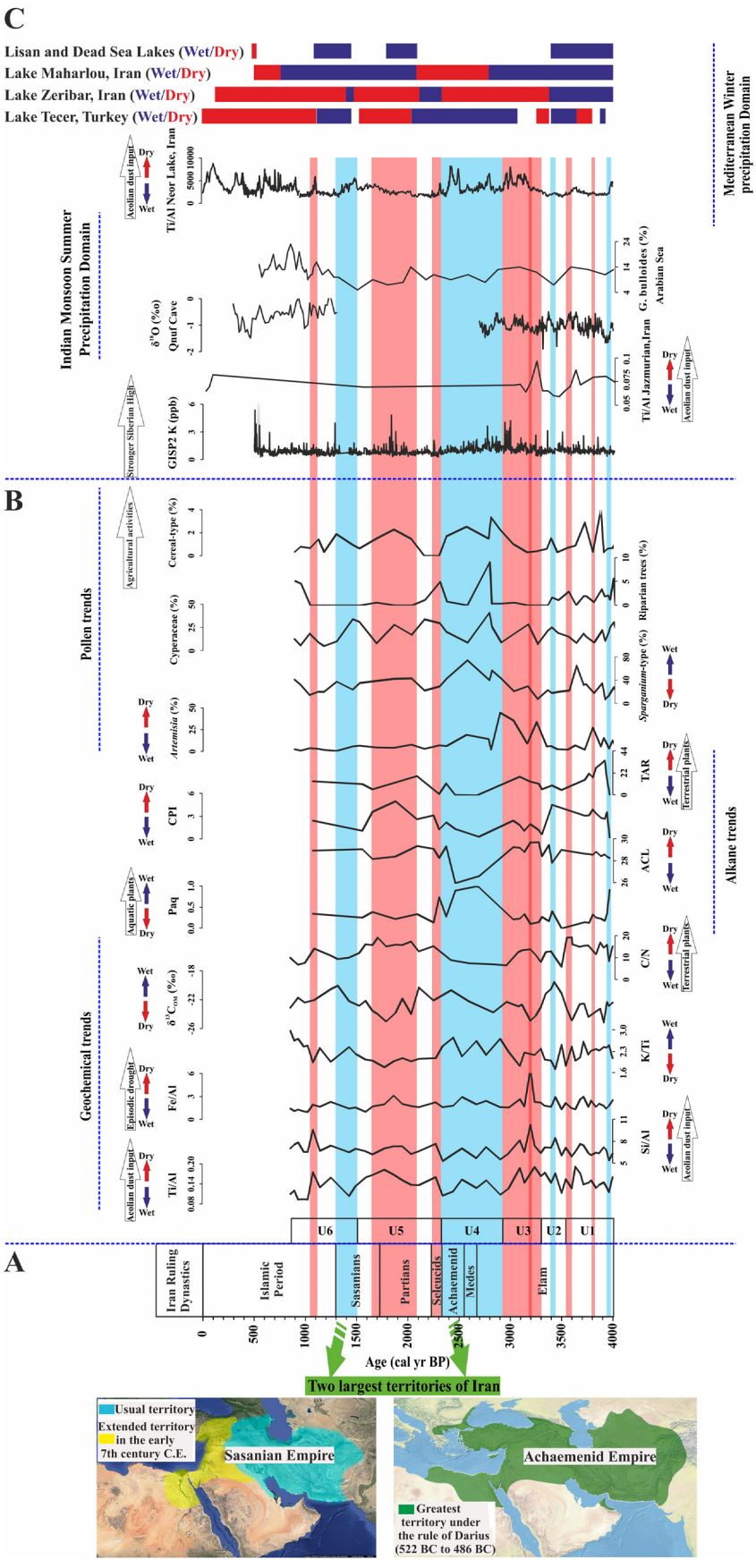

Fig. 3. Comparison of paleoclimate conditions inferred based on different proxies from the Jiroft peat sequence in southeastern Iran and other climate archives in west Asia and major ruling dynasties in Iran since the Early Bronze Age. A) Major ruling dynasties in Iran since the Early Bronze Age. The two wet periods coincide with the most extensive territories under the rules of the Achaemenid and Sasanian empires in Iran's imperial history (Mcdonough, 2011; Colburn, 2013). At its peak, the ancient Achaemenid Empire (c. 480 BCE) stretched 11 million km^2 which declined to 7.5 million km^2 during the Sassanid Empire c. 620 AD (Turchin et al., 2006). B) Selected sedimentology, geochemistry, and palynology results from the Jiroft peat sequence. C) Paleoclimate data from other sites indicating K concentrations in the GISP2 ice core as a proxy for changes in the strength of the Siberian Anticyclone (Mayewski et al., 1997); Ti/Al variations in the Jazmurian playa, SE Iran (Vaezi et al., 2019); Indian monsoon variation represented as $\delta^{18}O$ in a stalagmite from the Qunf Cave, Oman (Fleitmann et al., 2003); abundance of *Globigerina bulloides* from ODP Site 723, Arabian Sea (Gupta et al., 2003); Ti variations in Lake Neor, NW Iran, representing MLW intensity (Sharifi et al., 2015); and Compilation of Mesopotamian and Mediterranean palaeoclimate records (Migowski et al., 2006; Stevens et al., 2008; Djamali et al., 2009a; Kuzucuoğlu et al., 2011). The red and blue bars represent the dry and wet periods. (For interpretation of the references to colour in this figure legend, the reader is referred to the Web version of this article.)

Furthermore, the high P_{aq} (0.9) coeval with low CPI values imply waterlogging, which supports submerged/floating macrophytes in the peat (Meyers and Ishiwatari, 1993; Meyers, 1997).

The wet interval followed semi-wet conditions ca. 3900-3630 cal yr BP. This inference is consistent with the higher Si/Al and Ti/Al values. The peat has mid-range C/N and CPI values, indicating a mixture of higher terrestrial and aquatic plants. Consistent with this, the peat horizons indicate abundant trees, shrubs, and aquatic palynomorphs. Indeed, both emerging aquatic types of the Typhaceae family (*Sparganium*-type) and subaquatic/peat-forming taxa such as Cyperaceae present alternate peaks during this interval, even though with lower values. The abundance of Cerealia-type pollen counts at ca. 3880 to 3700 cal yr BP coincides with favorable climatic conditions for cereal agriculture.

Unit 2 (ca. 3550-3300 cal yr BP) is characterized by a distinct increase in $\delta^{13}C_{OM}$ coeval with a sharp drop in C/N ratios compared to Unit 1, indicating wet/semi-wet conditions. ACL values respond strongly to changes in water level, and the decrease in ACL is often linked to wet conditions (Cranwell, 1974; Schwark et al., 2002). Consistent with this, this unit's wet/semi-wet signal corresponds with low ACL values and higher values of Cyperaceae. Cerealia-type pollen has low values except for ca. 3400 cal yr BP, whereby high pollen counts accompany the high P_{aq} values. During this period, while Typhaceae decrease, *Artemesia* holds on before increasing towards the top of this unit. The less negative $\delta^{13}C_{OM}$ values in the peat suggest wet conditions and possibly even agricultural activities.

The time frame corresponding to Units 1 and 2 in the peat sequence aligns with a wet period in Lake Zeribar, NW Iran (Stevens et al., 2008; Wasylikowa and Witkowski, 2008). Similar wet conditions have been reported in the Jeita Cave, Lebanon (Verheyden et al., 2008). Consistent with our interpretation in this unit, an increase in humidity occurs in northern Syria between 4000 and 3750 cal yr BP (Fiorentino et al., 2008), and lacustrine isotope records in the eastern Mediterranean region between 3900 and 3700 cal yr BP. These changes suggest semi-wet conditions (Roberts et al., 2008). Stable isotope records from Mediterranean lakes show several enhanced wet episodes between 3900 and 3400 cal yr BP (Roberts et al., 2008). For example, humid conditions occur in Cappadocia, Turkey, ca. 3900 cal yr BP (Roberts et al., 2001). Similarly, the mineralogical and geochemical composition of sediments from Tecer Lake in central Turkey shows humid conditions ca. 3900 cal yr BP and between 3650 and 3400 cal yr BP (Kuzucuoğ;lu et al., 2011).

As described above, the paleoclimate conditions in the Jiroft Valley consist primarily of semi-wet and wet conditions. However, this period is punctuated by two short dry spells. The first short drought occurs ca. 3800 cal yr BP, as reflected by an increase in *Artemisia*. *Calligonum* and Ephedraceae pollen abundance are accompanied by a sharp decline of Typhaceae and Cerealia-type pollen in this interval. The second dry period occurs near the top of Unit 1 (ca. 3600-3550 cal yr BP). This dry period coincides with an increase in the Ti/Al ratio and is accompanied by low values of $\delta^{13}C_{OM}$ and high C/N ratios. The fall in TAR coincides with the sharp decrease in Typhaceae and Cerealia-type pollen. Gurjazkaite et al. (2018) indicated that the gyttja-dominated lithology in this section changed into amorphous peat around 3630-3550 cal yr BP, denoting a lower water table in the wetland and weathering from aerial exposure. The short dry period in this unit (Fig. 3) also coincides with the increase in aeolian input in the Jazmurian playa south of Konar Sandal (Vaezi et al., 2019). Likewise, a short drought ca. 3600 cal yr BP in northern Syria (Fiorentino et al., 2008) matches the sharp drop in the Dead Sea level (Migowski et al., 2006; Neumann et al., 2007).

5.2. The Late Bronze Age decline in Jiroft

In Unit 3 (164-134 cm; ca. 3300-2900 cal yr BP), deposition of coarse sand coupled with high Ti/Al and Si/Al ca. 3300 cal yr BP to 2900 cal yr BP (Fig. 3) represents high aeolian activity. This period covers a prolonged dry period with its peak around 3200 cal yr BP. Sediments deposited in this unit have distinct Rb/K and Fe/Al coupled with one of the lowest $\delta^{13}C_{OM}$ values indicative of arid conditions. The high ACL coeval with low P_{aq} values support the dominance of dry conditions in this interval. This arid period corresponds with the lowest values of *Sparganium*-type pollen. Notably, the highest counts of *Artemisia* in the entire peat sequence occur in this interval. In addition, desert shrubs (Ephedraceae and *Calligonum)* increase significantly, reflecting arid conditions, an increase in desertification, and the development of dunes (see Fig. 2, supplementary data). Cerealia-type pollen indicates the lowest counts (<1%) in this section, suggesting the near-disappearance of agricultural activities. This dry period was longer and more intense than previous dry intervals since 4000 cal yr BP. The dry and windy conditions in the Jiroft Valley are in agreement with an increase in K in the GISP2 ice core, Greenland, as an index of the Siberian Anticyclone strength (Mayewski et al., 1997) and a period of enhanced deposition of aeolian dust (coinciding with an increase of Ti) in Lake Neor, Iran (Sharifi et al., 2015). In Lake Maharlou (SW Iran), this period corresponds with low fluvial inputs and high deposition of evaporitic minerals (Brisset et al., 2018). Similar dry conditions have been reported in Lake Zeribar (western Iran) and marine sediment cores from the Mediterranean Sea (Schilman et al., 2001). (Kuzucuoğlu et al., 2011) reported a sharp decline in lake level, suggesting dry and arid conditions. Similarly, droughts have been reported in the Dead Sea ca. 3300-3000 cal yr BP (Kagan et al., 2015; Migowski et al., 2006) and Lake Van ca. 3300 cal yr BP (Lemcke and Sturm, 1997).

Similar arguments of climate change playing a causal role in the reduction of archeologically visible settlements (Cline, 2014) have been postulated for the Iranian plateau (and beyond into SE Asia) leading to the transition from Bronze Age to the Iron Age in the late second millennium BC. The dry, arid, and windy conditions in the Jiroft Valley are contemporaneous with the Late Bronze Age collapse in parts of Mesopotamia, the eastern Mediterranean region, and the southern Levant, coincided with socio-political upheaval and cultural decline (Weiss, 1982; Haggis, 1993; Kaniewski et al., 2010; Paulette, 2012; Langgut et al., 2013). For example, archaeological excavation from Ugarit near the modern city of Latakia, Syria, shows extreme heat and dryness ca. 3200 cal yr BP (Alpert and Neumann, 1989). In addition, Babylon reported crop failures, famine, and collapse based on textual and non-textual evidence from Mesopotamia between 3200 and 2900 cal yr BP (Neumann and Parpola, 1987). In the Tigris and Euphrates rivers, fluvial discharge declined, and famines were recorded in Mesopotamia and the eastern Mediterranean region (Kay and Johnson, 1981; Neumann and Parpola, 1987; Alpert and Neumann, 1989; Schilman et al., 2001). The steady decline in Northern and Southern Mesopotamia coincided with the end of the Assyrian dynasty and the eventual wane of Kassites (Sinha et al., 2019), with many communities adopting a more mobile and pastoral way of life as an adaptation to arid conditions and desertification (Paulette, 2012).

5.3. Rise and fall of the Persian Empire

In Unit 4 (134-106 cm; ca. 2900-2300 cal yr BP), high values of Si, Al, and K (see Fig. 1, supplementary data), coupled with the lowest aeolian inputs (as indicated by the low elemental ratios of Si/Al, Ti/Al, and high K/Ti), suggest the onset of wet conditions.

Consistent with this idea, this unit's increasing trend of $\delta^{13}C_{OM}$ coeval with low C/N ratios and the presence of long-chain *n*-alkanes support wet conditions and increased aquatic productivity. The sharp decline in ACL and CPI values contemporary with the highest P_{aq} in Unit 4 supports existing wet conditions. The dramatic decrease in *Artemisia* coupled with the increase in *Sparganium*-type pollen in this unit supports the prevailing wet conditions in the Jiroft valley. Unit 4 is also characterized by the highest and most continuous presence of Cerealia-type pollen, which is attributed to increased agricultural activities during wet conditions. Consistent with this trend in Jiroft, sediments in Lake Tecer, in central Turkey, suggest humid conditions existing between 2800 and 2000 cal yr BP (Kuzucuoğ;lu et al., 2011).

The time frame in unit 4 coincides with changes in the ruling dynasties of Iran. The Medes (ca. 2680-2550 cal yr BP) followed the collapse of the Elamite kingdom, and finally, the Achaemenid Empire rose (2550-2330 cal yr BP; Touraj, 2012; Colburn, 2013). The Achaemenid Empire, also called the First Persian Empire, was the largest empire in the ancient world, extending from Anatolia and Egypt across western Asia to northern India and Central Asia (Fig. 3). The Medes and Achaemenid rule coincided with large-scale agricultural activities in the Jiroft valley, as inferred from the significant appearance of Cerealia-type pollen (Fig. 3). Recent palynological studies indicate that agricultural practices expanded upland up to Lake Almalou (NW Iran) and in the southern Zagros region during the Achaemenid Empire (Djamali et al., 2016). The agro-pastoral activities flourished because of socioeconomic stability and the adoption of new methods for exploiting water resources and irrigation practices (Djamali et al., 2010b).

Our results show that it is possible that favorable climatic conditions supported socioeconomic stability and maintained the vast territory during the relatively long Achaemenid rule. Immediately above, Unit 5 (106-61 cm; ca. 2300-1550 cal yr BP) covers the decline of the Achaemenid Empire, followed by the Seleucids, and finally transitioning into the Parthian Empire, all the way up to the Sasanian Empire. The decline of the Achaemenid Empire (ca. 2300 cal yr BP) was coeval with dry conditions from ca. 2300-2240 cal yr BP at the beginning of this unit. Dry conditions at the beginning of this unit and immediately after the wet phase in the Jiroft valley are inferred based on the sharp decline in K and K/Ti and an increase in Ti/Al and Si/Al ratios. Moreover, the reduction in *Sparganium*-type pollen is coeval with the decrease of Cerealia-type pollen (almost absent for nearly 200 years between ca. 2300 and 2100 cal yr BP). Likewise, in other regions of Iran, Djamali et al. (2009a,b) reported that ca. 2350 cal yr BP, pollen counts for cultivated vegetation declined and are almost absent in Lake Almalou (NW Iran) and Lake Maharlou (in southern Iran). The authors speculate that the decrease in agricultural activities at the end of the Achaemenid Empire is most likely due to the destruction of infrastructure and temporary socioeconomic instability resulting from the invasions led by Alexander the Great (Djamali et al., 2010a,b). However, the dry conditions in the region coinciding with the collapse of the Achaemenid Empire indicate that climate change may also have been an underlying factor that made agricultural activities more marginal and could have triggered socioeconomic instability/unrest. It is possible that because of dry conditions, the communities that flourished along Halil Rud retreated and abandoned agriculture for nearly 200 years.

In Unit 5, K/Ti has low values compared to the high Ti/Al values. The maximum change happens between 2000 and 1530 cal yr BP implying high aeolian activity and dry conditions during this interval. Dry conditions are also inferred based on relatively lower *Sparganium*-type pollen counts than Unit 4. The lowest $\delta^{13}C_{OM}$ values in this section further support this interpretation. Significant increase in aeolian activity and dry conditions during this interval, especially between 2000 and 1650 cal yr BP, are consistent with a considerable rise of K in the GISP2 ice core, Greenland (Mayewski et al., 1997, Fig. 3) resulting from the positioning of the Siberian Anticyclone system over Iran (Mayewski et al., 1997). Similarly, dry conditions are suggested for the Lake Maharlou basin based on the Chenopodiaceae and *Artemisia* pollen counts ca. 1900 cal yr BP (Djamali et al., 2009a). After a hiatus in agricultural activities, the average value of Cerealia-type pollen increases a little (to around 1.74%) in the middle of this dry unit between 2000 and 1700 cal yr BP coinciding with the Parthian dynasty. This is the first time since 4000 cal yr BP that agriculture flourishes in the Jiroft valley despite arid conditions. It is likely that the increase of Cerealia-type pollen indicates the founding of new settlements in the Jiroft valley and cultural adaptation to farming under dry conditions.

5.3.1. The pre-Islamic period and recent times

At the beginning of Unit 6 (61-10 cm and extending from ca. 1550-850 cal yr BP), a sharp decrease in aeolian inputs occurs from ca. 1550-1300 cal yr BP. This is supported by the Ti/Al and high values of K/Ti coupled with low C/N and high $\delta^{13}C_{OM,}$ suggesting wet conditions in the Jiroft valley. The wet conditions are further evidenced by increased Typhaeae and Cerealia-type pollen. This second notable wet period since 4000 cal yr BP in the Jiroft valley is attributed to the inherent weakness of the Siberian High over Iran as inferred based on the major decrease in K concentration in the GISP2 ice core, Greenland (Mayewski et al., 1997, Fig. 3). Importantly, this wet period coincides with the second largest territorial boundaries in Iran's imperial history under the Sasanian Empire (ca. 1725-1300 cal yr BP; Daryaee, 2013). Agricultural activities increased in Northwestern Iran during the middle to late part of the Sasanian Empire, coinciding with wet conditions at the beginning of this unit (Djamali et al., 2010a,b; Shumilovskikh et al., 2017). Researchers have suggested that the expansion of farming probably happened because of socioeconomic stability and development in agricultural techniques (Djamali et al., 2010a,b; Shumilovskikh et al., 2017). Favorable climatic conditions supported the empire's economic prosperity and political stability.

After this wet interval, most parts of Unit 6 are characterized by moderate values of elemental ratios, indicating semi-wet conditions. The exception was the sediment horizon at ca. 1075 cal yr BP (34 cm), where high Si/Al and Ti/Al represent strong aeolian activity. In Unit 6, *Artemisia* counts are extremely low, and there is a moderate presence of *Sparganium*-type pollen, suggesting a semi-wet condition during this period. In addition, there are low Cerealia-type pollen counts from 1300 cal yr BP to the top of this unit. Previous studies indicate an overall political instability caused by weak successions and numerous invasions led by the Arabs, Turks, and Mongols during the post-Islamic period, which affected agricultural activities in the Iranian Plateau (Djamali et al., 2010a,b; Touraj, 2012). Furthermore, Sharifi et al. (2015) documented several short droughts with prominent levels of atmospheric dust deposited on the plateau since 1300 cal yr BP. The authors indicate that the collapse of the Sasanian empire ca. 1300 cal yr BP and the Safavid empire at 950 cal yr BP (Touraj, 2012; Daryaee, 2013) coincide with episodes of enhanced dust deposition in the Lake Neor record from NW Iran. The natural changes in the region triggered unrest associated with war, political tensions, and a socioeconomic crisis due to the scarcity of different resources. However, continued human occupation in the Jiroft Valley and southeastern Iran (and beyond) during such periods of climatic and environmental unpredictability was the flexibility of people to transition between various modes of subsistence and social organizations. This fact resonates unequivocally even in modern times at local or global scales.

6. Conclusions

A 2.5-m long peat sequence from the Jiroft Valley, covering the last 4000 cal yr BP, provides a unique, human-relevant climate record for southeastern Iran and helps us reconstruct past rainfall changes and vegetation patterns on the Iranian Plateau. Hydrological variations in the Jiroft Valley match similar trends in other MLW-dominated sites in the region. The hydroclimatic variations in the area since the Late Bronze Age are more related to the shifting of MLW and the northeast Siberian Anticyclone than IOSM variations. This trend continues even in modern times since IOSM has minimal influence on precipitation in this region. However, the proximity of the Jiroft Valley to the deserts made it overly sensitive to changes in rainfall in the past, with ramifications for agricultural activities and human settlements.

The first notable and significant appearance of Cerealia-type pollen in our record occurred ca. 3900-3700 cal yr BP coinciding with semi-wet climatic conditions in the Jiroft valley. The valley was dry and windy from 3300 to 2900 cal yr BP. The driest conditions in Jiroft during this arid interval occurred at ca. 3200 cal yr BP, coinciding with the collapse of the Late Bronze Age settlement in Konar Sandal. Notably, this close connection between agriculture and rainfall in this arid region set the stage for subsequent economic and political interactions. We show that two of the most powerful empires in Eurasian history, the Achaemenid and Sasanian Empires, are almost synchronous with the two wettest periods in our record. The trend suggests socioeconomic stability and the expansion of agricultural activities coeval with more favorable climatic conditions. Meanwhile, the decline of the Achaemenid Empire coincided with the beginning of a dry interval when, for nearly 200 years, agricultural practice in the Jiroft Valley was abandoned. Consistent with this trend, the decline in tree cover was reported in other regions of Iran, such as the catchments around Lake Almalou and Lake Maharlou.

Our data suggest that climate change can be considered one of the underlying factors affecting the major ruling dynasties in Iran, with climatic and environmental changes playing a significant role in agricultural sustainability and imperial provisioning on the Iranian Plateau. The changes in political power, economic networks, and military strength undoubtedly played significant roles in the development and fragmentation of the empires in this part of Eurasia. Nevertheless, we would argue that it is also essential to explore the role of climate change in the rise and ebb of imperial powers across space and time, with territorial control, trade, and exchange underpinned by agricultural practices in marginal environments. Future work should focus on developing more extensive archaeological understandings of changes in settlement patterns and farming practices alongside the exploration of records such as this, which can be related to different sites in the imperial heartlands of Iran.

Author contribution

JR conceived the idea and secured funding; he contributed to the lab and fieldwork, data interpretation, and writing. AV and MD led the lab work, writing, and data interpretation. KG helped with lab work. VT and ANB helped with fieldwork and writing. PR helped with writing and data interpretation.

Declaration of competing interest

The authors declare that they have no known competing financial interests or personal relationships that could have appeared to influence the work reported in this paper.

Data availability

Data will be made available on request.

Acknowledgments

We are very thankful for the support extended by INIOAS during the field campaign. In particular, the authors thank Naser Ghasemi and Mohammed Ali Hamzeh for their support and Parisa Habibi for help in the magnetic susceptibility measurements. We also thank Susanne Karlsson, Mårten Dario, Lena Lundman, and Kasun Gayantha for their support. This research was funded by Vetenskapsrådet grant E0402601 to JR. PR would like to thank the Max Planck Society for funding.

Appendix A. Supplementary data

Supplementary data to this article can be found online at https://doi.org/10.1016/j.quascirev.2022.107855.

References

Agnew, A.D.Q., Zohary, M., 1974. Geobotanical foundations of the Middle East. J. Ecol. 62, 349–350. https://doi.org/10.2307/2258907.

Allan, J., Douglas, A.G., 1977. Variations in the content and distribution of n-alkanes in a series of Carboniferous vitrinites and sporinites of bituminous rank. Geochem. Cosmochim. Acta 41, 1223–1230.

Alpert, P., Neumann, J., 1989. An ancient "Correlation" between streamflow and distant rainfall in the near East. J. Near East. Stud. 48, 313–314. https://doi.org/10.1086/373411.

Aubert, C., Brisset, E., Djamali, M., Sharifi, A., Ponel, P., Gambin, B., Akbari Azirani, T., Guibal, F., Lahijani, H., Naderi Beni, A., de Beaulieu, J.-L., Pourmand, A., Andrieu-Ponel, V., Thiéry, A., Gandouin, E., 2017. Late glacial and early Holocene hydroclimatic variability in northwest Iran (Talesh Mountains) inferred from chironomid and pollen analysis. J. Paleolimnol. 58, 151–167.

Blaauw, M., Andrés Christen, J., 2011. Flexible paleoclimate age-depth models using an autoregressive gamma process. Bayesian Analysis 6, 457–474. https://doi.org/10.1214/11-BA618.

Bourbonniere, R.A., Meyers, P.A., 1996. Sedimentary geolipid records of historical changes in the watersheds and productivities of Lakes Ontario and Erie. Limnol. Oceanogr. 41, 352–359. https://doi.org/10.4319/lo.1996.41.2.0352.

Brisset, E., Djamali, M., Bard, E., Borschneck, D., Gandouin, E., Garcia, M., Stevens, L., Tachikawa, K., 2019. Late Holocene hydrology of Lake Maharlou, southwest Iran, inferred from high-resolution sedimentological and geochemical analyses. J. Paleolimnol. 61, 111–128. https://doi.org/10.1007/s10933-018-0048-6.

Calvert, S.E., Fontugne, M.R., 2001. On the late Pleistocene—Holocene sapropel record of climatic and oceanographic variability in the eastern Mediterranean. Paleoceanography 16, 78–94.

Clarke, J., et al., 2016. Climatic changes and social transformations in the Near East and North Africa during the 'long' 4th millennium BC: a comparative study of environmental and archaeological evidence. Quat. Sci. Rev. 136, 96–121. https://doi.org/10.1016/j.quascirev.2015.10.003.

Cline, E.H., 2014. In 1177 BC: the Year Civilization Collapsed. Princeton University Press.

Colburn, H.P., 2013. Connectivity and communication in the Achaemenid empire 1. J. Econ. Soc. Hist. Orient 56, 29–52. https://doi.org/10.1163/15685209-12341278.

Cranwell, P.A., 1974. Monocarboxylic acids in lake sediments: indicators, derived from terrestrial and aquatic biota of paleoenvironmental trophic levels. Chem. Geol. 14, 1–14. https://doi.org/10.1016/0009-2541(74)90092-8.

Cranwell, P.A., Eglinton, G., Robinson, N., 1987. Lipids of aquatic organisms as potential contributors to lacustrine sediments—II. Org. Geochem. 11, 513–527.

Daryaee, T., 2013. In: Sasanian Persia the Rise and Fall of an Empire, Paperback. I.B.Tauris & Co Ltd, London, p. 256.

Dehghani, M., Djamali, M., Gandouin, E., Akhani, H., 2017. A pollen rain-vegetation study along a 3600 m mountain-desert transect in the Irano-Turanian region; implications for the reliability of some pollen ratios as moisture indicators. Rev. Palaeobot. Palynol. 247, 133–148. https://doi.org/10.1016/j.revpalbo.2017.08.004.

Dixit, Y., Hodell, D.A., Sinha, R., Petrie, C.A., 2014. Abrupt weakening of the Indian summer monsoon at 8.2 kyr B.P. Earth Planet Sci. Lett. 391, 16–23.

Djamali, M., Beaulieu, J.-L.De, Miller, N.F., Andrieu-Ponel, V., Ponel, P., Lak, R., Sadeddin, N., Akhani, H., Fazeli, H., 2009a. Vegetation history of the SE section of the Zagros Mountains during the last five millennia; a pollen record from the Maharlou Lake, Fars Province. Iran. Veg. Hist. Archaeobot 18, 123–136.

Djamali, M., Beaulieu, J.-L.De, Andrieu-Ponel, V., Berberian, M., Miller, N.F., Gandouin, E., Lahijani, H., Shah-Hosseini, M., Ponel, P., Salimian, M., Guiter, F.,

2009b. A late Holocene pollen record from Lake Almalou in NW Iran: evidence for changing land-use in relation to some historical events during the last 3700 years. J. Archaeol. Sci. 36, 1364–1375.
Djamali, M., Akhani, H., Andrieu-Ponel, V., Braconnot, P., Brewer, S., de Beaulieu, jacques, L., Fleitmann, D., Fleury, J., Gasse, F., Guibal, F., Jackson, S., Lezine, A.-M., Médail, F., Ponel, P., Roberts, N., Stevens, L., 2010a. Indian Summer Monsoon variations could have affected the early-Holocene woodland expansion in the Near East. Holocene 20, 813–820. https://doi.org/10.1177/0959683610362813.
Djamali, M., Jones, M.D., Migliore, J., Balatti, S., Fader, M., Contreras, D., Gondet, S., Hosseini, Z., Lahijani, H., Naderi, A., Shumilovskikh, L.S., Tengberg, M., Weeks, L., 2016. Olive cultivation in the heart of the Persian Achaemenid Empire: new insights into agricultural practices and environmental changes reflected in a late Holocene pollen record from Lake Parishan, SW Iran. Veg. Hist. Archaeobotany 25, 255–269. https://doi.org/10.1007/s00334-015-0545-8.
Djamali, M., Kürschner, H., Akhani, H., de Beaulieu, J.-L., Amini, A., Andrieu-Ponel, V., Ponel, P., Stevens, L., 2008. Palaeoecological significance of the spores of the liverwort Riella (Riellaceae) in a late Pleistocene long pollen record from the hypersaline Lake Urmia, NW Iran. Rev. Palaeobot. Palynol. 152, 66–73.
Djamali, M., Miller, N.F., Ramezani, E., Andrieu-Ponel, V., de Beaulieu, J.-L., Berberian, M., Guibal, F., Lahijani, H., Lak, R., Ponel, P., 2010b. Notes on arboricultural and agricultural practices in ancient Iran based on new pollen evidence. Paleorient 36, 175–188. https://doi.org/10.3406/paleo.2010.5394.
Eglinton, G., Hamilton, R.J., 1967. Leaf epicuticular waxes: the waxy outer surfaces of most plants display a wide diversity of fine structure and chemical constituents. Science 156, 1322–1335. https://doi.org/10.1126/science.156.3780.1322.
Emami, M., Razani, M., Soleimani, N.A., Madjidzadeh, Y., 2017. New insights into the characterization and provenance of chlorite objects from the Jiroft civilization in Iran. J. Archaeol. Sci. Reports 16, 194–204. https://doi.org/10.1016/j.jasrep.2017.10.004.
Enzel, Y., Ely, L.L., Mishra, S., Ramesh, R., Amit, R., Lazar, B., Rajaguru, S.N., Baker, V.R., Sandler, A., 1999. High-resolution Holocene environmental changes in the thar desert, northwestern India. Science 284, 125–128.
Fallah, B., Sodoudi, S., Russo, E., Kirchner, I., Cubasch, U., 2015. Towards modeling the regional rainfall changes over Iran due to the climate forcing of the past 6000 years. Quat. Int. 429, 1–10.
Faraji, F., Ashja-Ardalan, A., Kalimi-Noghreeian, M., Jafari, H., 2019. Study of types of texture in intrusive masses in Northeast of Jiroft. Dilemas contemporáneos. Educación, política y valores 6, 1–18.
Ficken, K.J., Li, B., Swain, D.L., Eglinton, G., 2000. An n-alkane proxy for the sedimentary input of submerged/floating freshwater aquatic macrophytes. Org. Geochem. 31, 745–749. https://doi.org/10.1016/S0146-6380(00)00081-4.
Fiorentino, G., Caracuta, V., Calcagnile, L., D'Elia, M., Matthiae, P., Mavelli, F., Quarta, G., 2008. Third millennium B.C. climate change in Syria highlighted by Carbon stable isotope analysis of ^{14}C—AMS dated plant remains from Ebla. Palaeogeogr. Palaeoclimatol. Palaeoecol. 266, 51–58. https://doi.org/10.1016/j.palaeo.2008.03.034.
Fleitmann, D., Burns, S.J., Mudelsee, M., Neff, U., Kramers, J., Mangini, A., Matter, A., 2003. Holocene forcing of the Indian monsoon recorded in a stalagmite from southern Oman. Science 300, 1737–1739.
Fouache, E., Cosandey, C., Adle, C., Casanova, M., Francfort, H., Madjidzadeh, Y., Tengberg, M., Sajadi, M., Shirazi, Z., Vahdati, A., 2009. A study of the climatic crisis of the end of the Third millennium BC in Southeastern Iran through the lens of geomorphology and archaeology. EGU General Assembly Conference Abstracts 1505.
Fouache, E., Garçon, D., Rousset, D., Sénéchal, G., Madjidzadeh, Y., 2005. La vallée de l'Halil Roud (région de Jiroft, Iran) : étude géoarchéologique, méthodologie et résultats préliminaires. Paleorient 31, 107–122. https://doi.org/10.3406/paleo.2005.5128.
Goslar, T., Czernik, J., Goslar, E., 2004. Low-energy ^{14}C AMS in Poznań radiocarbon laboratory, Poland. Nucl. Instrum. Methods Phys. Res. Sect. B Beam Interact. Mater. Atoms 223, 5–11. https://doi.org/10.1016/j.nimb.2004.04.005.
Gupta, A.K., Anderson, D.M., Overpeck, J.T., 2003. Abrupt changes in the Asian southwest monsoon during the Holocene and their links to the North Atlantic Ocean. Nature 421, 354–357.
Gurjazkaite, K., Routh, J., Djamali, M., Vaezi, A., Poher, Y., Beni, A.N., Tavakoli, V., Kylin, H., 2018. Vegetation history and human-environment interactions through the late Holocene in Konar Sandal, SE Iran. Quat. Sci. Rev. 194, 143–155. https://doi.org/10.1016/j.quascirev.2018.06.026.
Haggis, D.C., 1993. Intensive survey, traditional settlement patterns, and dark age crete: the case of early Iron age kavousi. J. Mediterr. Archaeol. 6, 131–174. https://doi.org/10.1558/jmea.v6i2.131.
Hamzeh, M.A., Mahmudy Gharaie, M.H., Alizadeh Ketek Lahijani, H., Djamali, M., Moussavi Harami, R., Naderi Beni, A., 2016. Holocene hydrological changes in SE Iran, a key region between Indian Summer Monsoon and Mediterranean winter precipitation zones, as revealed from a lacustrine sequence from Lake Hamoun. Quat. Int. 408, 25–39. https://doi.org/10.1016/j.quaint.2015.11.011.
Hedges, J.I., Stern, J.H., 1984. Carbon and nitrogen determinations of carbonate-containing solids1. Limnol. Oceanogr. 29, 657–663. https://doi.org/10.4319/lo.1984.29.3.0657.
Jiang, H., Ding, Z., 2010. Eolian grain-size signature of the sikouzi lacustrine sediments (Chinese loess plateau): implications for neogene evolution of the east asian winter monsoon. GSA Bull 122, 843–854.
Kagan, E.J., Langgut, D., Boaretto, E., Neumann, F.H., Stein, M., 2015. Dead Sea levels during the Bronze and Iron ages. Radiocarbon 57, 237–252. https://doi.org/10.2458/azu_rc.57.18560.
Kaniewski, D., Paulissen, E., Van Campo, E., Weiss, H., Otto, T., Bretschneider, J., Van Lerberghe, K., 2010. Late second-early first millennium BC, abrupt climate changes in coastal Syria and their possible significance for the history of the Eastern Mediterranean. Quat. Res. 74, 207–215. https://doi.org/10.1016/j.yqres.2010.07.010.
Kay, P.A., Johnson, D.L., 1981. Estimation of Tigris-Euphrates streamflow from regional paleoenvironmental proxy data. Clim. Change 3, 251–263.
Kuzucuoğlu, C., Dörfler, W., Kunesch, S., Goupille, F., 2011. Mid- to late-Holocene climate change in central Turkey: the Tecer lake record. Holocene 21, 173–188. https://doi.org/10.1177/0959683610384163.
Langgut, D., Finkelstein, I., Litt, T., 2013. Climate and the Late Bronze collapse: new evidence from the southern Levant. Tel Aviv 40, 149–175.
Laskar, A.H., Bohra, A., 2021. Impact of Indian summer monsoon change on ancient Indian civilizations during the Holocene. Front. Earth Sci. 663. https://doi.org/10.3389/feart.2021.709455.
Lemcke, G., Sturm, M., 1997. δ^{18}O and trace element measurements as proxy for the reconstruction of climate changes at Lake Van (Turkey): preliminary results. In: H, N., Kukla, G., Weiss, H. (Eds.), Third Millennium BC Climate Change and Old World Collapse. Springer Berlin Heidelberg, Berlin, Heidelberg, pp. 653–678. https://doi.org/10.1007/978-3-642-60616-8_29.
Leonard, J., 1993. Comparisons between the phytochorological spectra of three Iranian deserts and those of various surrounding regions. Bull. du Jard. Bot. Natl. Belgique/Bull. Natl. Plant. Belg. 62, 389–396. https://doi.org/10.2307/3668284.
Madella, M., Fuller, D.Q., 2006. Palaeoecology and the harappan civilisation of south Asia: a reconsideration. Quat. Sci. Rev. 25, 1283–1301.
Madjidzadeh, Y., Pittman, H., 2008. Excavations at konar sandal in the region of Jiroft in the Halil basin: first preliminary report (2002–2008). Iran 46, 69–103. https://doi.org/10.1080/05786967.2008.11864738.
Mancini-Lander, D.J., 2009. A history of Iran. Am. J. Islam Soc. 26, 121–123. https://doi.org/10.35632/ajis.v26i4.1371.
Martinez-Ruiz, F., Kastner, M., Gallego-Torres, D., Rodrigo-Gámiz, M., Nieto-Moreno, V., Ortega-Huertas, M., 2015. Paleoclimate and paleoceanography over the past 20,000 yr in the Mediterranean Sea Basins as indicated by sediment elemental proxies. Quat. Sci. Rev. 107, 25–46.
Mashkour, M., Tengberg, M., Shirazi, Z., Madjidzadeh, Y., 2013. Bio-archaeological studies at konar sandal, Halil Rud basin, southeastern Iran. Environ. Archaeol. 18, 222–246.
Mayewski, P.A., Meeker, L.D., Twickler, M.S., Whitlow, S., Yang, Q., Lyons, W.B., Prentice, M., 1997. Major features and forcing of high latitude northern hemisphere atmospheric circulation using a 110,000 year long glaciochemical series. J. Geophys. Res. Ocean. 102, 26345–26366.
Mcdonough, S., 2011. The legs of the throne: kings, elites and subjects in sasanian Iran. In: Arnason, J.P., Raaflaub, K.A. (Eds.), The Roman Empire in Context: Historical and Comparative Perspectives, pp. 290–321. https://doi.org/10.1002/9781444390186.ch13.
Mercone, D., Thomson, J., Abu-Zied, R.H., Croudace, I.W., Rohling, E.J., 2001. High-resolution geochemical and micropalaeontological profiling of the most recent eastern Mediterranean sapropel. Mar. Geol. 177, 25–44.
Meyers, P.A., 1997. Organic geochemical proxies of paleoceanographic, paleolimnologic, and paleoclimatic processes. Org. Geochem. 27, 213–250. https://doi.org/10.1016/S0146-6380(97)00049-1.
Meyers, P.A., Ishiwatari, R., 1993. Lacustrine organic geochemistry—an overview of indicators of organic matter sources and diagenesis in lake sediments. Org. Geochem. 20, 867–900. https://doi.org/10.1016/0146-6380(93)90100-.
Migowski, C., Stein, M., Prasad, S., Negendank, J.F.W., Agnon, A., 2006. Holocene climate variability and cultural evolution in the Near East from the Dead Sea sedimentary record. Quat. Res. 66, 421–431. https://doi.org/10.1016/j.yqres.2006.06.010.
Neumann, F.H., Kagan, E.J., Schwab, M.J., Stein, M., 2007. Palynology, sedimentology and palaeoecology of the late Holocene Dead Sea. Quat. Sci. Rev. 26, 1476–1498. https://doi.org/10.1016/j.quascirev.2007.03.004.
Neumann, J., Parpola, S., 1987. Climatic change and the eleventh-tenth-century eclipse of Assyria and Babylonia. J. Near E. Stud. 46, 161–182. https://doi.org/10.1086/373244.
Njagi, D.M., Routh, J., Olago, D., Gayantha, K., 2021. A multi—proxy reconstruction of the late Holocene climate evolution in the Kapsabet Swamp, Kenya (East Africa). Palaeogeogr. Palaeoclimatol. Palaeoecol. 574, 110475. https://doi.org/10.1016/j.palaeo.2021.110475.
Paulette, T., 2012. Domination and resilience in Bronze age Mesopotamia. In: Cooper, J., Sheets, P. (Eds.), Surviving Sudden Environmental Change: Answers from Archaeology, vol. 167. University Press of Colorado, p. 196. https://doi.org/10.2307/j.ctt1wn0rbs.12.
Petrie, C.A., Weeks, L., 2019. The Iranian plateau and the Indus river basin. In: Chiotis, E. (Ed.), Climate Change in the Holocene - Impacts and Human Adaptations. CRC Press, Boca Raton, Florida.
Ponton, C., Giosan, L., Eglinton, T.I., Fuller, D.Q., Johnson, J.E., Kumar, P., Collett, T.S., 2012. Holocene aridification of India. Geophys. Res. Lett. 39. https://doi.org/10.1029/2011GL050722.
Pyankova, L., 1994. Central Asia in the Bronze age: sedentary and nomadic cultures. Antiquity 68, 355–372. https://doi.org/10.1017/S0003598X00046718.
Reimer, P.J., Austin, W.E.N., Bard, E., Bayliss, A., Blackwell, P.G., Bronk Ramsey, C., Butzin, M., Cheng, H., Edwards, R.L., Friedrich, M., Grootes, P.M., Guilderson, T.P., Hajdas, I., Heaton, T.J., Hogg, A.G., Hughen, K.A., Kromer, B., Manning, S.W., Muscheler, R., Palmer, J.G., Pearson, C., Van Der Plicht, J., Reimer, R.W., Richards, D.A., Scott, E.M., Southon, J.R., Turney, C.S.M., Wacker, L., Adolphi, F.,

Büntgen, U., Capano, M., Fahrni, S.M., Fogtmann-Schulz, A., Friedrich, R., Köhler, P., Kudsk, S., Miyake, F., Olsen, J., Reinig, F., Sakamoto, M., Sookdeo, A., Talamo, S., 2020. The IntCal20 northern hemisphere radiocarbon age calibration curve (0-55 cal kBP). Radiocarbon 62, 725–757. https://doi.org/10.1017/RDC.2020.41.

Roberts, N., Jones, M.D., Benkaddour, A., Eastwood, W.J., Filippi, M.L., Frogley, M.R., Lamb, H.F., Leng, M.J., Reed, J.M., Stein, M., 2008. Stable isotope records of Late Quaternary climate and hydrology from Mediterranean lakes: the ISOMED synthesis. Quat. Sci. Rev. 27, 2426–2441.

Roberts, N., Reed, J.M., Leng, M.J., Kuzucuoğlu, C., Fontugne, M., Bertaux, J., Woldring, H., Bottema, S., Black, S., Hunt, E., Karabiyikoğlu, M., 2001. The tempo of Holocene climatic change in the eastern Mediterranean region: new high-resolution crater-lake sediment data from central Turkey. Holocene 11, 721–736. https://doi.org/10.1191/09596830195744.

Safaierad, R., Mohtadi, M., Zolitschka, B., Yokoyama, Y., Vogt, C., Schefuß, E., 2020. Elevated dust depositions in West Asia linked to ocean-atmosphere shifts during North Atlantic cold events. Proc. Natl. Acad. Sci. USA 117, 18272–18277. https://doi.org/10.1073/pnas.2004071117.

Schilman, B., Bar-Matthews, M., Almogi-Labin, A., Luz, B., 2001. Global climate instability reflected by Eastern Mediterranean marine records during the late Holocene. Palaeogeogr. Palaeoclimatol. Palaeoecol. 176, 157–176. https://doi.org/10.1016/S0031-0182(01)00336-4.

Schwark, L., Zink, K., Lechterbeck, J., 2002. Reconstruction of postglacial to early Holocene vegetation history in terrestrial Central Europe via cuticular lipid biomarkers and pollen records from lake sediments. Geology 30, 463–466.

Sharifi, A., Pourmand, A., Canuel, E.A., Ferer-Tyler, E., Peterson, L.C., Aichner, B., Feakins, S.J., Daryaee, T., Djamali, M., Beni, A.N., Lahijani, H.A.K., Swart, P.K., 2015. Abrupt climate variability since the last deglaciation based on a high-resolution, multi-proxy peat record from NW Iran: the hand that rocked the Cradle of Civilization? Quat. Sci. Rev. 123, 215–230. https://doi.org/10.1016/j.quascirev.2015.07.006.

Shirani, M., Afzali, K.N., Jahan, S., Strezov, V., Soleimani-Sardo, M., 2020. Pollution and contamination assessment of heavy metals in the sediments of Jazmurian playa in southeast Iran. Sci. Rep. 10, 1–11. https://doi.org/10.1038/s41598-020-61838-x.

Shumilovskikh, L., Djamali, M., Andrieu-Ponel, V., Ponel, P., de Beaulieu, J.-L., Naderi-Beni, A., Sauer, E.W., 2017. Palaeoecological insights into agri-horti-cultural and pastoral practices before, during and after the sasanian empire. In: Sasanian Persia: between Rome and the Steppes of Eurasia, second ed. Edinburgh University Press, Edinburgh, pp. 51–73.

Sinha, A., Kathayat, G., Weiss, H., Li, H., Cheng, H., Reuter, J., Schneider, A.W., Berkelhammer, M., Adali, S.F., Stott, L.D., Lawrence Edwards, R., 2019. Role of climate in the rise and fall of the neo-Assyrian empire. Sci. Adv. 5, eaax6656. https://doi.org/10.1126/sciadv.aax6656.

Staubwasser, M., Weiss, H., 2006. Holocene climate and cultural evolution in late prehistoric–early historic west Asia. Quat. Res. 66, 372–387. https://doi.org/10.1016/j.yqres.2006.09.001.

Stevens, L.R., Ito, E., Wright, H.E., 2008. Variations in effective moisture at Lake Zeribar, Iran during the last glacial period and Holocene, inferred from the $\delta^{18}O$ values of authigenic calcite. In: Wasylikowa, K., Witkowski, A. (Eds.), Diatom Monographs, Vol. 8, the Palaeoecology of Lake Zeribar and Surrounding Areas, Western Iran, During the Last 48,000 Years. A.R.G. Gantner Verlag K.G., p. 377

Stuiver, H.A., Pollach, M., 1977. Reporting of ^{14}C data: a discussion. Radiocarbon 19.

Touraj, D., 2012. The Oxford Handbook of Iranian History. Oxford University Press, Oxford.

Turchin, P., Adams, J.M., Hall, T.D., 2006. East-West orientation of historical empires and Modern States. J. World Syst. Res. https://doi.org/10.5195/jwsr.2006.369.

Vaezi, A., Ghazban, F., Tavakoli, V., Routh, J., Beni, A.N., Bianchi, T.S., Curtis, J.H., Kylin, H., 2019. A Late Pleistocene-Holocene multi-proxy record of climate variability in the Jazmurian playa, southeastern Iran. Palaeogeogr. Palaeoclimatol. Palaeoecol. 514, 754–767. https://doi.org/10.1016/j.palaeo.2018.09.026.

Verheyden, S., Nader, F.H., Cheng, H.J., Edwards, L.R., Swennen, R., 2008. Paleoclimate reconstruction in the Levant region from the geochemistry of a Holocene stalagmite from the Jeita cave, Lebanon. Quat. Res. 70, 368–381. https://doi.org/10.1016/j.yqres.2008.05.004.

Vidale, M., Frenez, D., 2015. Indus components in the iconography of a white marble cylinder seal from Konar Sandal South (Kerman, Iran). J. SE Asian Studies 31, 144e154.

Wasylikowa, E.K., Witkowski, A. (Eds.), 2008. Diatom Monographs Vol.8 the Palaeoecology of Lake Zeribar and Surrounding Areas, Western Iran, during the Last 48000 Years. A.R.G. Gantner Verlag.

Wehausen, R., Brumsack, H.J., 2000. Chemical cycles in Pliocene sapropel-bearing and sapropel-barren eastern Mediterranean sediments. Palaeogeogr. Palaeoclimatol. Palaeoecol. 158, 325–352.

Weiss, B., 1982. The decline of Late Bronze Age civilization as a possible response to climatic change. Clim. Change 4, 173–198. https://doi.org/10.1007/BF02423389.

Weiss, H., Courty, M.-A., Wetterstrom, W., Guichard, F., Senior, L., Meadow, R., Curnow, A., 1993. The genesis and collapse of third millennium north Mesopotamian civilization. Science 261, 995–1004.

White, F., Léonard, J., 1991. Phytogeographical links between Africa and southwest Asia. Flora et vegetatio. Mundi 9, 229–246.

Zandifar, S., Tavakoli, V., Vaezi, A., Naeimi, M., Naderi Beni, A., Sharifi-Yazdi, M., Routh, J., 2022. Influence of transport mechanism on playa sequences, late Pleistocene-Holocene period in Jazmurian Playa, southeast Iran. Arabian J. Geosci. 15. https://doi.org/10.1007/s12517-022-09918-2.

Zhang, P., Cheng, H., Edwards, R.L., Chen, F., Wang, Y., Yang, X., Liu, Jian, Tan, M., Wang, X., Liu, Jinghua, An, C., Dai, Z., Zhou, J., Zhang, D., Jia, J., Jin, L., Johnson, K.R., 2008. A test of climate, sun, and culture relationships from an 1810 year Chinese cave record. Science 322, 940–942.